Title: SPACE: spatially resolved multiomic analysis for high-throughput CRISPR screening in 3D models

Mengwei Hu[1]†, Yi Cui[2]†, Qianhui Huang[1], Khoi Chu[1], Sierra McKinzie[2], Michael Patrick[2], Sharanya Iyengar[1], Maerjianghan Abuduli[1], Marianne Spatz[1], Nandita Joshi[1], Brendan Miller[1], Shams Vellarikkal[1], Timothy Riordan[2], Danny Bitton[1], Jan Lubojacky[1], Iya Khalil[1], Federica Piccioni[1], Michael Rhodes[2], Alex Tamburino[1], Shanshan He[2], Joseph Beechem[2], Vanessa Peterson[1]*

†These authors contributed equally to this work.
*Corresponding author

Affiliation:

[1]Merck & Co., Inc., Rahway, NJ, USA

[2]Bruker Spatial Biology, Seattle, WA

Abstract

SPAtial Cell Exploration (**SPACE**) is a novel subcellular imaging-based method that couples large-scale perturbations with whole transcriptome single-cell multi-omics readout, while preserving spatial context, providing unprecedented insights into tissue organization and microenvironmental interactions at very low cost. As a demonstration, we performed SPACE in hundreds of spheroids and discovered novel biology related to CAF-tumor interactions using unbiased approaches. This scalable, cost-effective technology has broad applications in translational research and drug discovery, offering a transformative approach to high-throughput spatial perturbation studies.

Introduction

The ability to systematically perturb cellular models while maintaining spatial context is essential for understanding complex tissue biology. Traditional single-cell approaches, such as Perturb-seq, provide high-dimensional readouts but require dissociation of cells from their native microenvironment, limiting our ability to study cell-cell interactions and spatial organization. To overcome these limitations, recent technique advancements have led to multiple spatial CRISPR screen technologies of different phenotypic modalities[1-8]. However, one limitation in the field is that the readouts are often focused on a targeted panel of pre-selected RNA/proteins derived from specific hypotheses, restraining the scope of novel biological discovery. To further expand the data plexity of spatial CRISPR screen, extend its application to 3D models and realize hypothesis-free biological discovery, we introduce SPAtial Cell Exploration (SPACE), a novel imaging-based method of perturbation readout that enables high-throughput, single-cell resolution multi-omic profiling at whole transcriptome scale, while preserving spatial context in complex 3D models.

SPACE integrates whole-transcriptome measurements, CRISPR identity detection, and protein expression analysis within intact cellular models, providing a comprehensive view of cellular responses to perturbations. Unlike sequencing-based approaches, which can be cost-prohibitive at scale and lose the native spatial environment, SPACE significantly reduces the cost of whole-transcriptome profiling, allowing for high-throughput perturbation studies across large-scale 3D model systems such as spheroids,

assembloids, and organoids. As a demonstration, we profiled CRISPR perturbations in hundreds of spheroids (containing close to 70,000 total cells) in a cost-effective approach which would have been prohibitive at scale using conventional sequencing methods.

SPACE enables direct visualization of spatially resolved receptor-ligand interactions, eliminating the need to infer cell-cell communication from dissociated single cells. This ability to pinpoint which cells are adjacent and actively engaging in molecular signaling provides unprecedented insights into tissue organization and cellular crosstalk. Our findings establish SPACE as the first imaging-based method that enables perturbation and whole-transcriptome-level readout on the same slide while retaining spatial resolution and offering a scalable and cost-effective approach for high-content cellular perturbation studies.

Results & Discussion:

To demonstrate the feasibility of spatially resolved CRISPR identity detection in single cells, we first used CosMx to detect guide RNA (gRNA) sequences and a unique gRNA identifier (UGI) in a pool of lentivirus-infected cells that constitutively express CRISPR gRNA/UGI (Figure S1). We detected on average 9.5304 gRNA copies and 18.6305 UGI copies per cell. The strong correlation between the gRNA and UGI counts per cell (Figure. S1D) suggested high detection specificity, resulting in confident CRISPR identity assignment in close to 75% of cells (Figure. S1E). These data suggested that CosMx successfully decodes CRISPR identities in a pool of 2D cell culture.

To enable SPACE technology in 3D models, we utilized a co-culture system of cancer-associated fibroblasts (CAF) and tumor cells, which has been widely used in studying CAF-tumor crosstalk and anticancer drug screening[9]. We CRISPR edited the CAFs in 96-well format, with each well containing pairs of gRNAs and corresponding UGIs for demultiplexing CRISPR identity. We then co-cultured CRISPR-edited CAFs and tumor cells in ultra-low attachment plates to allow the spheroid formation while maintaining the well positions of each CRISPR edit as a reference for evaluating spatial CRISPR detection accuracy (Figure 1A).

For SPACE CRISPR detection, we designed CosMx probes targeting both gRNAs and their UGIs. We coupled spatial CRISPR detection with either 6K or whole-transcriptome (WTX) CosMx RNA profiling and protein markers to assist cell segmentation (Figure 1B). Using adjacent sections, we confirmed the spatial distribution of CAFs and tumor cells via H&E and COMET staining (Figure S2). With SPACE, we generated high dimensional multi-modal data of hundreds of CRISPR-edited CAF-tumor spheroids, enabling unbiased discovery on CAF-tumor interaction post CAF CRISPR editing.

To evaluate SPACE assay performance in the spheroid model, we prepared spheroids edited in 42 genes plus negative control *AAVS1*, and performed SPACE of 6K RNA + CRISPR gRNA/UGI on 2 slides with 93 spheroids per slide (Figure S3). The detected gene counts per cell highly correlate between the two replicates with an R^2=0.996, with on average 851 unique genes and 1445 RNA counts per cell, demonstrating robust endogenous mRNA detection (Figure S3A). To assess SPACE CRISPR detection performance, we quantified the count per spheroid for each gRNA and UGI, and ranked them from highest to lowest, respectively. The most abundant gRNA or UGI detected in each spheroid consistently correspond to the expected CRISPR perturbation and far surpass the copy numbers of unexpected CRISPR molecules by at least 4 fold (Figure S3B and C), allowing us to confidently decode CRISPR identities with the “highest expressing” gRNA and UGI for each spheroid.

-Bruker Confidential-

To expand SPACE RNA detection coverage to WTX while retaining the ability to decode CRISPR identity, we performed SPACE using CosMx WTX RNA panel with or without CRISPR molecule profiling (Figure S4). We detected an average of 1518 unique genes and 2188 transcripts per cell with WTX+CRISPR, which is highly comparable to an average of 1516 genes and 2405 transcripts per cell with WTX-only. The gene counts are highly correlated between WTX-only and WTX+CRISPR with R^2=0.928 (Figure S4A). Compared with 6K+CRISPR experiment, WTX+CRISPR achieved a 78% increase in mean unique genes per cell and a 51% increase in mean transcripts per cell. These data demonstrated that CRISPR molecule detection is highly compatible with WTX RNA profiling without severely impacting WTX RNA detection.

The SPACE CRISPR detection performance was highly consistent between 6K+CRISPR and WTX+CRISPR, with R^2=0.759 when comparing gRNA counts and R^2=0.662 when comparing UGI counts (Figure S4B), indicating that SPACE CRISPR detection is highly robust to a wide range of RNA detection plexity. In WTX+CRISPR, the most abundant gRNA or UGI in each spheroid also agreed with the ground truth and counted at least 6-fold higher than unexpected CRISPR molecules (Figure S4C and D), allowing confident CRISPR identity assignment. With refined cell segmentation (Figure S5), we confidently identified CAF and tumor populations based on the expression levels of marker genes, such as collagen genes and *FAP* for CAF lineage[10], and *KRT5* and *KRT17*[11] for tumor lineage (Figure 1C-E and Figure S6). In summary, our data demonstrated that SPACE enables highly robust transcript profiling and accurate CRISPR identity detection in 3D models, and is compatible with a wide range of RNA plexity up to whole-transcriptome scale.

The high-dimensional perturbation profiling data generated by SPACE allowed us to unbiasedly explore gene functions in CAF-tumor interplay. By analyzing differentially expressed genes between CAFs with different gene KOs compared to *AAVS1*-KO, we found that CAF *ISG20* KO profoundly reduced the expression level of multiple matrix metalloproteinase (MMP) family genes in CAFs and increased the expression level of known MMP inhibitors (Figure 2A and Figure S7). MMPs are crucial in remodeling extracellular matrix (ECM) and regulating tumor progression and metastasis[12]. Reactome Pathway analysis also revealed that *ISG20*-KO spheroids displayed significant depletion of pathways related to MMP activity (Figure 2B). We further confirmed the downregulation of MMP1 expression in *ISG20*-KO CAFs via RNAscope (Figure 2C). These data suggest that SPACE robustly detects transcriptome changes caused by CRISPR edits, enabling confident discovery of novel biology at scale.

Tumor cell density has been shown to regulate various cancer behaviors such as metastasis[13]. The effect of cell density on gene expression caused by gene perturbations has also been observed in other spatial CRISPR screens, such as Perturb-FISH[4]. To explore if the observed MMP pathway activity in CAF is affected by its surrounding cell density, we categorized CAF cells into low-tumor-density and high-tumor-density groups based on their neighboring tumor cell counts (see Methods), and compared their MMP pathway activity in different gene KO spheroids. Interestingly, we found that in the control *AAVS1*-KO spheroids, low-tumor-density CAFs exhibited higher MMP pathway activity than high-tumor-density CAFs, which was not seen in *ISG20*-KO spheroids (Figure 2D). The SPACE technology allows spatially resolved CRISPR screen in 3D spheroid models, providing a method to dissect the delicate interplay between gene expression of each single cell and its surrounding environment, which is not possible with sequencing methods using dissociated cells.

The ECM is an important and integral component of tumor microenvironment and mediates the crosstalk between CAF and tumor[10]. ECM proteins, such as fibronectin and collagen, can bind to receptors on tumor cell surface and influence cell growth and migration[14]. We suspected that the CRISPR edits in CAFs may alter the ligand-receptor (LR) interactions between CAF and tumor and thus reshape tumor

-Bruker Confidential-

transcriptome. We reasoned that because LR interaction is more likely to happen between spatially adjacent cells, incorporating the spatial information embedded in our SPACE dataset into LR analysis will increase the confidence in finding true LR interactions, compared to the non-spatially-informed LR analysis. By performing unbiased LR analysis with spatial refinement, we identified the top LR pairs that are spatially enriched or depleted at CAF-tumor interface for each CRISPR edited spheroid (Figure 2E). Notably, *ISG20*-KO spheroids displayed increased interaction between CAF collagens and tumor CD44 (Figure 2E and F), potentially related to its reduced MMP pathway activity and consequently less collagen degradation. We also found that *RNF213*-KO spheroids display stronger interaction between CAF and tumors through various ECM proteins and cell adhesion molecules, including collagen, fibronectin, integrins and SDC4 (Figure 2E and F). In line with that strong ECM connections through integrins can activate proliferative signaling pathway in tumor[14], the tumor cells in *RNF213*-KO spheroids showed increased activity in many pathways related to cell division and proliferation, including chromosome segregation and nucleosome assembly and organization (Figure S8A). Besides direct LR interaction between CAF and tumor cells, ECM could be reshaped by altered cell metabolism indirectly[15]. With SPACE, we found that tumor cells in CAF *APOL6*-KO spheroids, a gene involved in lipid metabolism, exhibited reduced activity in TGF-β signaling (Figure S8B) and upregulated expression level of *TP53AIP1* (Figure S8C), indicating an intricate connection between energy metabolism and tumor phenotype.

SPACE enabled unbiased identification of spatially variable genes (SVGs) that are specific to certain gene edits, which potentially indicates previously unknown mechanisms of gene regulation and cell-cell interaction in mixed cell population. By performing SVG analysis, we found a spatially coordinated 5-gene signature in *GBP4*-KO spheroids (Figure 2G and Figure S9). *GBP4* is an interferon-stimulated gene that can negatively regulate type-I interferon signaling[16], a pathway with complex roles in cancer[17]. Interestingly, GBP4 is among the most abundant GBP family proteins in pancreatic cancer, and is associated with poor prognosis in pancreatic cancer patients[18]. Among the gene signature, *IFNA10* is a member of type-I interferon, and *AQP5* and *ZNF132* have been indicated to be potential prognostic markers in various cancer types[19, 20]. Further investigation is needed to dissect the relationship between *GBP4* and the 5-gene signature in interferon signaling and CAF-tumor interplay.

Lastly, to further unleash the multimodal potential of SPACE and thoroughly utilize the rich phenotypic landscape offered by spatial CRISPR screening, we demonstrated SPACE detection of WTX transcriptome, CRISPR identities, and multiplexed protein of up to 68 markers, all on the same slide (Figure S10A and B). Similar to the WTX+CRISPR experiments, the multimodal SPACE successfully identified CAF and tumor populations (Figure S10C and D). As a proof of concept, this is the highest-plex multi-modal CRISPR screen that has ever been accomplished to our knowledge. The incorporation of multiplexed protein detection into multimodal SPACE will enable hypothesis-free discovery of novel perturbation biology at scale with unprecedented ability to completely profile the downstream effects of genomic perturbation.

In summary, SPACE enabled high-throughput spatial profiling of transcriptome, protein and CRISPR perturbations at single-cell resolution. By performing SPACE on hundreds of CRISPR-edited spheroids, we achieved unbiased and systematic discovery of gene function on stromal and cancer biology, and uncovered novel biological insights across different aspects of CAF-tumor interplay. SPACE reaches the state-of-the-art of current single cell and spatial CRISPR screen platforms, with its unprecedented transcriptome coverage, high protein plexity, and compatibility with FFPE and 3D models (Table S1). SPACE can be further expanded to other types of high-throughput screens, including CRISPRa/i, pooled perturbation, and chemical or small molecule perturbation. The comprehensive perturbation dataset

-Bruker Confidential-

generated by SPACE will also be a valuable resource for generative AI/ML models to learn, predict and unify human causal biology[3]. By applying SPACE to different translational models with high-throughput perturbations and further multiplexing of multimodal phenotypic readouts, we envision SPACE will accelerate biomedical research and discoveries via its ability to demultiplex perturbations and visualize phenome at a cost-effective manner.

-Bruker Confidential-

Figure 1: SPACE workflow in spheroid model.
A: Diagram of SPACE experimental workflow. Primary cancer associated fibroblasts (CAF) are CRISPR edited, co-cultured with BxPC3 cancer cells in ultra-low attachment plates to allow spheroid formation, and fixed. The spheroids are then embedded in FFPE blocks while maintaining 96-well arrayed format for CRISPR identity confirmation. The sectioned slides undergo SPACE profiling of CRISPR molecules, transcriptome and protein on the same slide. Created in BioRender.

B: Example images from SPACE workflow. Left: morphological staining of whole slide containing 93 spheroids placed in arrayed format. Scale bar: 1 mm. Top right: Morphological staining markers. Scale bar: 100 µm. Bottom right: composite images of representative spheroids, showing different synthetic gRNAs, *COL1A1* mRNA, PanCK protein and nuclear staining. Scale bar: 150 µm.

C: Cell clustering using endogenous mRNAs detected by SPACE.

D: Expression level of marker genes for CAF/tumor annotation in each cluster.

E: Cell clustering with cell type of CAF and tumor annotated.

Figure 2: SPACE enables unbiased novel discovery of CAF-tumor interplay.
A: Volcano plot of differentially expressed genes of CAFs in *ISG20*-KO vs *AAVS1*-KO spheroids with selected MMP pathway-related genes labeled.

B: Reactome pathway analysis of *ISG20*-KO spheroids compared to *AAVS1*-KO spheroids.

C: MMP1 downregulation in *ISG20*-KO spheroids compared to *AAVS1*-KO spheroids. From top to bottom, each row represents the results of: CAF *MMP1* RNA expression level from WTX+CRISPR SPACE, CAF (represented by PCK-/Vimentin+) *MMP1* RNA median intensity from RNAscope, CAF MMP1 protein median intensity from RNAscope, respectively. From left to right, each column represents the results of: violin plots of MMP1 expression in *AAVS1*-KO (red) and *ISG20*-KO (teal) spheroids, representative images of *AAVS1*-KO spheroids, representative images of *ISG20*-KO spheroids, respectively. P values were calculated by Wilcoxon rank-sum test. Scale bar: 100 µm.

D: Relationship between local tumor density at CAF and CAF MMP pathway activity. The top row represents data from *AAVS1*-KO spheroids and bottom row represents *ISG20*-KO spheroids. From left to right, each column represents: MMP pathway activity between CAFs with low tumor density (<0.003 tumor cells/μm^2) versus high tumor density, spheroid heatmap of local tumor density at CAFs, and spheroid heatmap of MMP pathway activity in CAFs. Tumor cells are visualized in gray color in the heatmaps. P values were calculated by Wilcoxon two-sided rank-sum test.

E: LR score differences between the spatially informed vs nonspatially informed analysis for each CRISPR edits (blue – high LR interaction score in nonspatially informed analysis; red – high LR interaction score in spatially informed analysis). Only LR pairs identified in more than 5 KO conditions are presented. Black boxes highlighted *ISG20*-KO and *RNF213*-KO spheroids.

F: Chord diagrams showing the spatially informed LR pairs specific to ISG20 KO and RNF213 KO spheroids compared to nonspatially informed analysis (LR pairs with score difference > 0). The arc length of each LR pair represents its weight among all identified LR pairs.

-Bruker Confidential-

G: Waterfall plot of median SVG score for the 5-gene signature in each CRISPR edits and SVG score heatmap of selected spheroids.

Figure S1: CosMx detection of CRISPR identities in a pool of lentivirus-infected cells.
A: Diagram of experimental workflow. Cells are infected in separate wells by lentivirus that express different combinations of gRNAs and their corresponding UGIs, and selected for puromycin resistance. The cells expressing different gRNAs/UGIs are then pooled and seeded onto chamber slides, fixed, and continued with CosMx workflow. Figure created with Biorender.

B: CosMx lentivirus vector design. The construct was modified from CROP-seq vectors. Briefly, the gRNA expression cassette (human U6 promoter – gRNA – tracr) is embedded in the 3'LTR, downstream of Puromycin resistance gene and WPRE that are driven by EF-1α promoter. A 50-basepair UGI is inserted between WPRE and 3'LTR.

C: RNAscope detection of CRISPR molecules in cells expressing B2M gRNA and UGI. Left: detecting B2M UGI (yellow). Middle: detecting tracrRNA (magenta). Right: detecting CD81 UGI (yellow). Scale bar: 20 µm.

D: CosMx detection of CRISPR molecules in mixed cell pools (left column) and correlation between the gRNA and UGI counts of the same gene (right column). Examples are shown for two gRNAs, TREM2 (up) and MERTK (down). Scale bar: 100 µm.

E: Decoding CRISPR identity in mixed cell pool by CosMx-detected UGI. Up: Pie chart of cell decoding results. Down: CosMx image of UGI distribution in the cell pool. Scale bar: 50 µm.

Figure S2: H&E and COMET staining of SPACE spheroid array.
A: H&E staining.

B: COMET protein staining showing selective markers: DAPI, Vimentin and KRT14.

Figure S3: SPACE assay performance with 6K RNA panel.
A: Gene expression correlation between two slides in a 6K+CRISPR SPACE assay. Each dot represents the log-transformed (log1p) total count of the gene within the dataset.

B: Total counts per spheroid of the top 5 most abundant synthetic gRNAs in selected spheroid. Left: *AAVS1*-KO spheroids; right: *ISG20*-KO spheroids.

C: Total counts per spheroid of the top 5 most abundant UGIs in selected spheroid. Left: *AAVS1*-KO spheroids; right: *ISG20*-KO spheroids.

-Bruker Confidential-

Figure S4: SPACE assay performance with WTX RNA panel.
A: Gene expression correlation between WTX+CRISPR experiment (x axis) and WTX-only experiment (y axis).

B: Correlation of detected CRISPR molecule count between WTX+CRISPR (x axis) and 6K+CRISPR (y axis). Left: gRNA count correlation; right: UGI count correlation.

C: Total counts per spheroid of the top 5 most abundant gRNAs in selected spheroid. Left: *AAVS1*-KO spheroids; right: *ISG20*-KO spheroids.

D: Total counts per spheroid of the top 5 most abundant UGIs in selected spheroid. Left: *AAVS1*-KO spheroids; right: *ISG20*-KO spheroids.

Figure S5: Example of cell segmentation.
Channels of DAPI, histone and PanCK protein staining were used for segmentation.

A: DAPI.

B: Histone.

C: PanCK.

D: Composite with segmentation mask shown.

Scale bar: 50 µm.

Figure S6: Cell type clustering of CAF-tumor spheroid.
Expression level of marker genes in each cluster.

Figure S7: MMP downregulation in *ISG20*- vs *AAVS1*-KO spheroids.
Violin plots of selected gene expression level in CAFs in *AAVS1*-KO and *ISG20*-KO spheroids quantified from WTX+CRISPR SPACE. P values were calculated by Wilcoxon rank sum test.

Figure S8: Differentially expressed genes in tumor.
A: Enriched GO terms (biological process) of upregulated tumoral genes.

B: Enriched GO terms (biological process) of downregulated tumoral genes.

C: Volcano plot of differentially expressed genes in tumor cells of *APOL6*-KO spheroids.

Figure S9: Spatially variable gene module in *GBP4*-KO spheroids.

-Bruker Confidential-

Representative images from SPACE showing the RNAs of the 5-gene SVG in AAVS1-KO and GBP4-KO spheroids. Scale bar: 50 µm.

Figure S10: Multimodal SPACE.
A: Representative images of RNA detection of multiomic SPACE. Selective transcripts and morphological markers for cell segmentation are shown for the same *ORMDL3*-KO spheroid. Scale bar: 50 µm.

B: Representative images of protein detection of multiomic SPACE. Selective protein stainings are shown for the same spheroid as A. Scale bar: 50 µm.

C: Cell clustering of multiomic SPACE based on endogenous mRNAs.

D: Expression level of selected marker genes across different cell clusters.

Table S1: Comparison between SPACE and other single cell/spatial perturbation technologies.

Table S2: gRNA and UGI sequences for CosMx CRISPR identity detection in lentivirus-infected cell pool.

Table S3: gRNAs and their corresponding UGI sequences for SPACE in CAF-tumor spheroids.

Table S4: CosMx probe design of CRISPR identity detection in lentivirus-infected cell pool.

Table S5: SPACE probe design of CRISPR identity detection in spheroids.

Acknowledgements: We thank Heather Zhou (Merck & Co., Inc., Rahway, NJ, USA), Meagan Sullender (Merck & Co., Inc., Rahway, NJ, USA), the Broad Functional Genomics Consortium and UMass Medical School Gene Therapy Center for their help in designing the lentivirus vectors and generating lentiviruses. We thank Erin Piazza (Bruker) for help with RNA ISH probe design.

Author contributions:

Conceived and designed the study: V.P.

Performed experiment: M.H., S.M., K.C., M.A. with the help from S.I. CosMx CRISPR guide/barcode Probe designed by T.R. UGIs designed by D.B. and J.L.

Analyzed the data: Y.C., Q.H., M.P. with the help from B.M., N.J., S.V.

Supervised the study: V.P., S.H., J.B., A.T., M.R., M.S., F.P., I.K.

Wrote the manuscript: M.H., Y.C., V.P. (with input from all authors).

-Bruker Confidential-

321 **Figure 1**

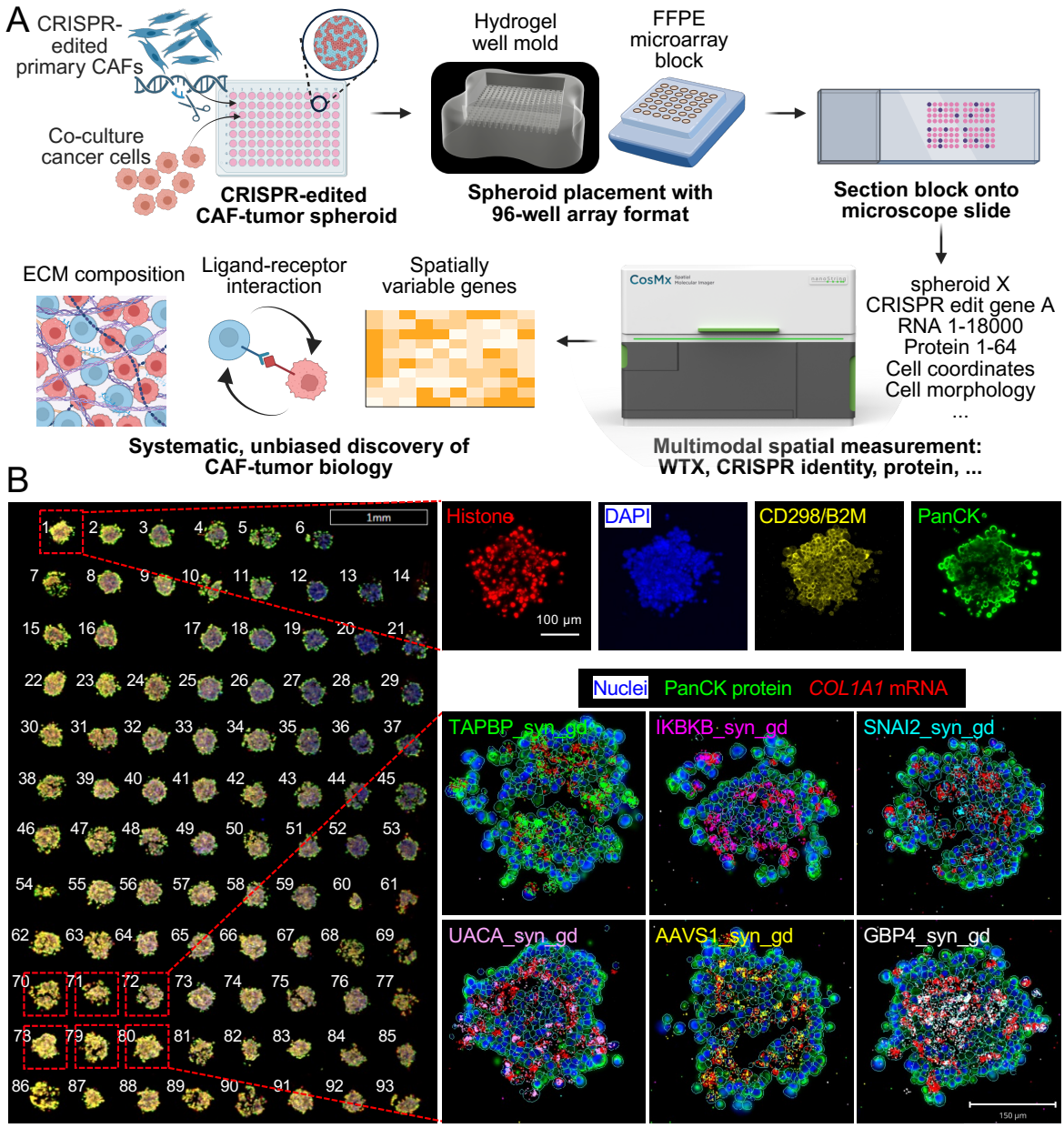

322

-Bruker Confidential-

Figure 1: SPACE workflow in spheroid model

A: Diagram of SPACE experimental workflow. Primary cancer associated fibroblasts (CAF) are CRISPR edited, co-cultured with BxPC3 cancer cells in ultra-low attachment plates to allow spheroid formation, and fixed. The spheroids are then embedded in FFPE blocks while maintaining 96-well arrayed format for CRISPR identity confirmation. The sectioned slides undergo SPACE profiling of CRISPR molecules, transcriptome and protein on the same slide. Created in BioRender.

B: Example images from SPACE workflow. Left: morphological staining of whole slide containing 93 spheroids placed in arrayed format. Scale bar: 1 mm. Top right: Morphological staining markers. Scale bar: 100 µm. Bottom right: composite images of representative spheroids, showing different synthetic gRNAs, *COL1A1* mRNA, PanCK protein and nuclear staining. Scale bar: 150 µm.

C: Cell clustering using endogenous mRNAs detected by SPACE.

D: Expression level of marker genes for CAF/tumor annotation in each cluster.

E: Cell clustering with cell type of CAF and tumor annotated.

-Bruker Confidential-

337 **Figure 2**

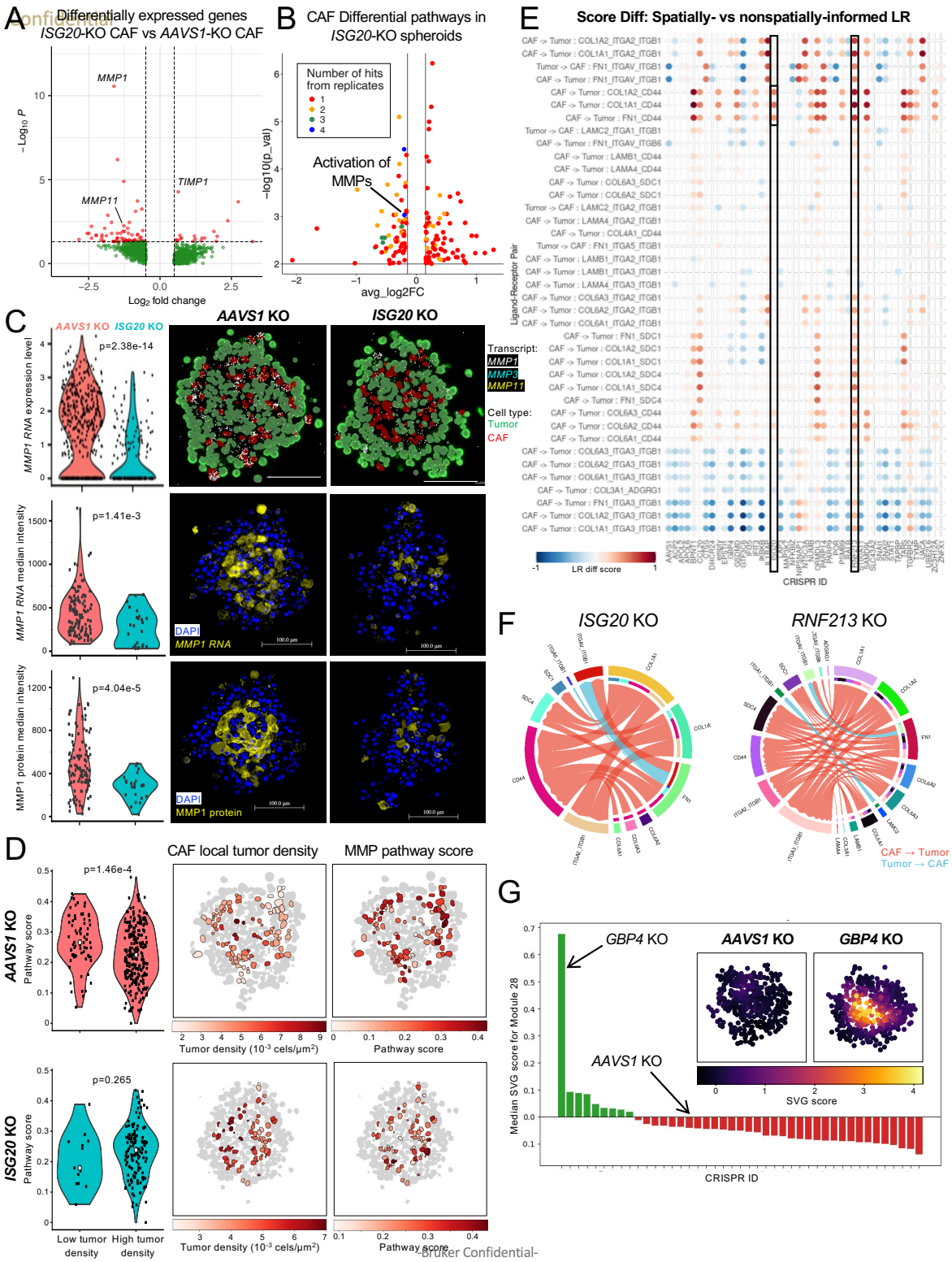

-Bruker Confidential-

338

-Bruker Confidential-

Figure 2: SPACE enables unbiased novel discovery of CAF-tumor interplay

A: Volcano plot of differentially expressed genes of CAFs in *ISG20*-KO vs *AAVS1*-KO spheroids with selected MMP pathway-related genes labeled.

B: Reactome pathway analysis of *ISG20*-KO spheroids compared to *AAVS1*-KO spheroids.

C: MMP1 downregulation in *ISG20*-KO spheroids compared to *AAVS1*-KO spheroids. From top to bottom, each row represents the results of: CAF *MMP1* RNA expression level from WTX+CRISPR SPACE, CAF (represented by PCK-/Vimentin+) *MMP1* RNA median intensity from RNAscope, CAF MMP1 protein median intensity from RNAscope, respectively. From left to right, each column represents the results of: violin plots of MMP1 expression in *AAVS1*-KO (red) and *ISG20*-KO (teal) spheroids, representative images of *AAVS1*-KO spheroids, representative images of *ISG20*-KO spheroids, respectively. P values were calculated by Wilcoxon rank-sum test. Scale bar: 100 µm.

D: Relationship between local tumor density at CAF and CAF MMP pathway activity. The top row represents data from *AAVS1*-KO spheroids and bottom row represents *ISG20*-KO spheroids. From left to right, each column represents: MMP pathway activity between CAFs with low tumor density (<0.003 tumor cells/μm^2) versus high tumor density, spheroid heatmap of local tumor density at CAFs, and spheroid heatmap of MMP pathway activity in CAFs. Tumor cells are visualized in gray color in the heatmaps. P values were calculated by Wilcoxon two-sided rank-sum test.

E: LR score differences between the spatially informed vs nonspatially informed analysis for each CRISPR edits (blue – high LR interaction score in nonspatially informed analysis; red – high LR interaction score in spatially informed analysis). Only LR pairs identified in more than 5 KO conditions are presented. Black boxes highlighted *ISG20*-KO and *RNF213*-KO spheroids.

F: Chord diagrams showing the spatially informed LR pairs specific to ISG20 KO and RNF213 KO spheroids compared to nonspatially informed analysis (LR pairs with score difference > 0). The arc length of each LR pair represents its weight among all identified LR pairs.

-Bruker Confidential-

364 **Figure S1**

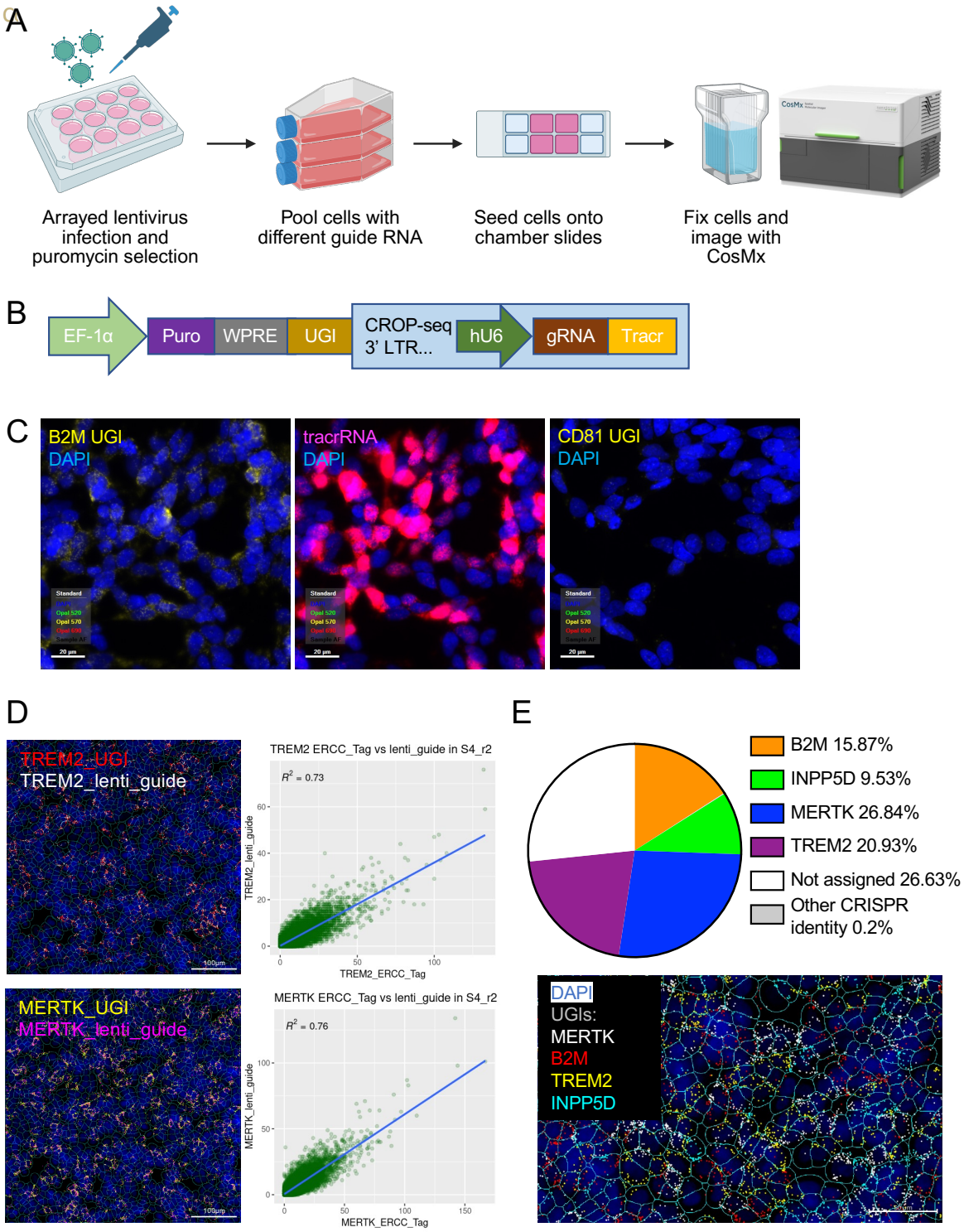

-Bruker Confidential-

365

-Bruker Confidential-

366 Figure S1: CosMx detection of CRISPR identities in a pool of lentivirus-infected cells

367 A: Diagram of experimental workflow. Cells are infected in separate wells by lentivirus that express
368 different combinations of gRNAs and their corresponding UGIs, and selected for puromycin resistance.
369 The cells expressing different gRNAs/UGIs are then pooled and seeded onto chamber slides, fixed, and
370 continued with CosMx workflow. Figure created with Biorender.

371 B: CosMx lentivirus vector design. The construct was modified from CROP-seq vectors. Briefly, the
372 gRNA expression cassette (human U6 promoter – gRNA – tracr) is embedded in the 3'LTR, downstream
373 of Puromycin resistance gene and WPRE that are driven by EF-1α promoter. A 50-basepair UGI is
374 inserted between WPRE and 3'LTR.

375 C: RNAscope detection of CRISPR molecules in cells expressing B2M gRNA and UGI. Left: detecting
376 B2M UGI (yellow). Middle: detecting tracrRNA (magenta). Right: detecting CD81 UGI (yellow). Scale
377 bar: 20 µm.

378 D: CosMx detection of CRISPR molecules in mixed cell pools (left column) and correlation between the
379 gRNA and UGI counts of the same gene (right column). Examples are shown for two gRNAs, TREM2
380 (up) and MERTK (down). Scale bar: 100 µm.

381 E: Decoding CRISPR identity in mixed cell pool by CosMx-detected UGI. Up: Pie chart of cell decoding
382 results. Down: CosMx image of UGI distribution in the cell pool. Scale bar: 50 µm.

383

-Bruker Confidential-

Figure S2

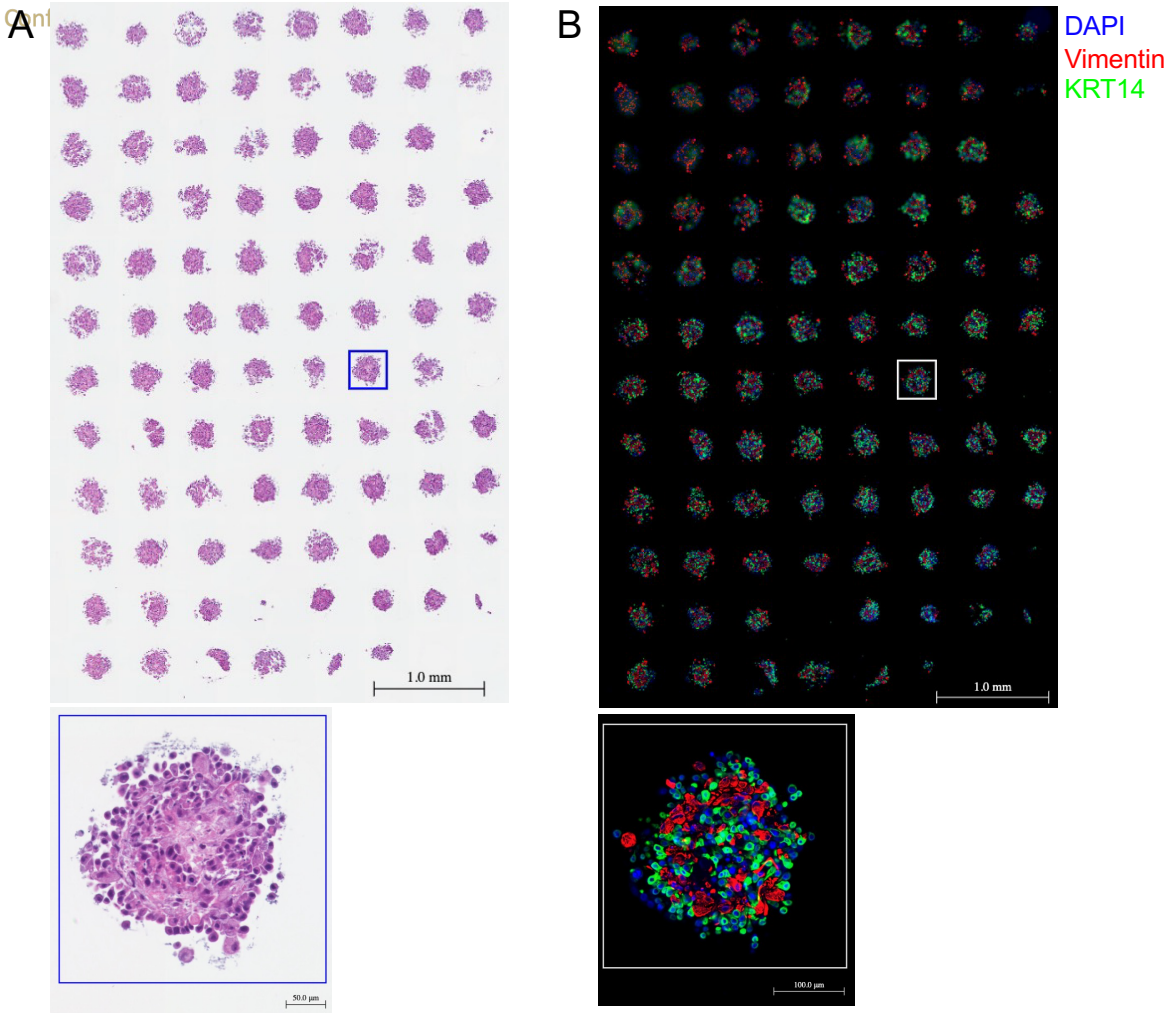

Figure S2: H&E and COMET staining of SPACE spheroid array

A: H&E staining.

B: COMET protein staining showing selective markers: DAPI, Vimentin and KRT14.

Figure S3

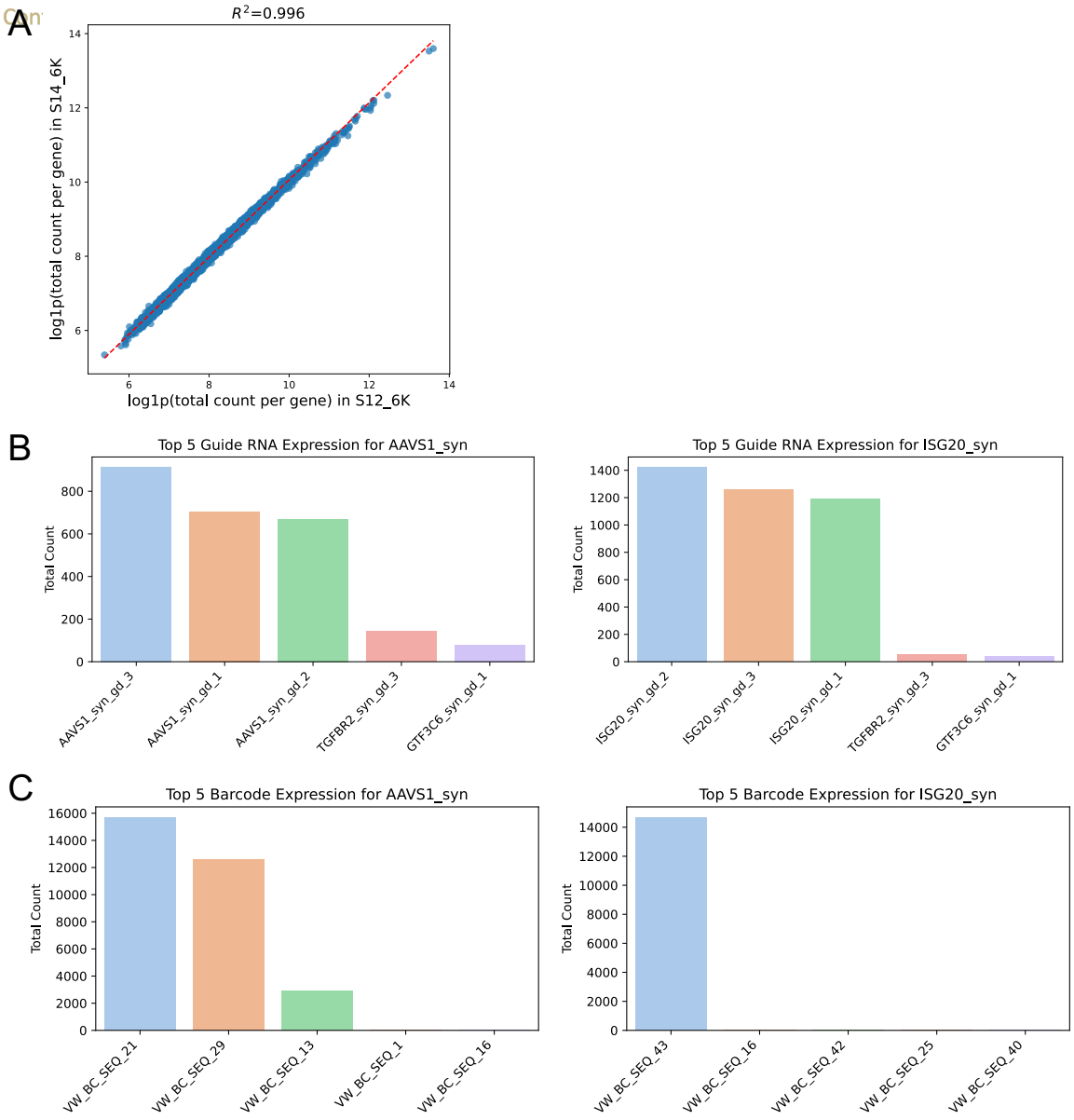

Figure S3: SPACE assay performance with 6K RNA panel

A: Gene expression correlation between two slides in a 6K+CRISPR SPACE assay. Each dot represents the log-transformed (log1p) total count of the gene within the dataset.

B: Total counts per spheroid of the top 5 most abundant synthetic gRNAs in selected spheroid. Left: *AAVS1*-KO spheroids; right: *ISG20*-KO spheroids.

C: Total counts per spheroid of the top 5 most abundant UGIs in selected spheroid. Left: *AAVS1*-KO spheroids; right: *ISG20*-KO spheroids.

-Bruker Confidential-

Figure S4

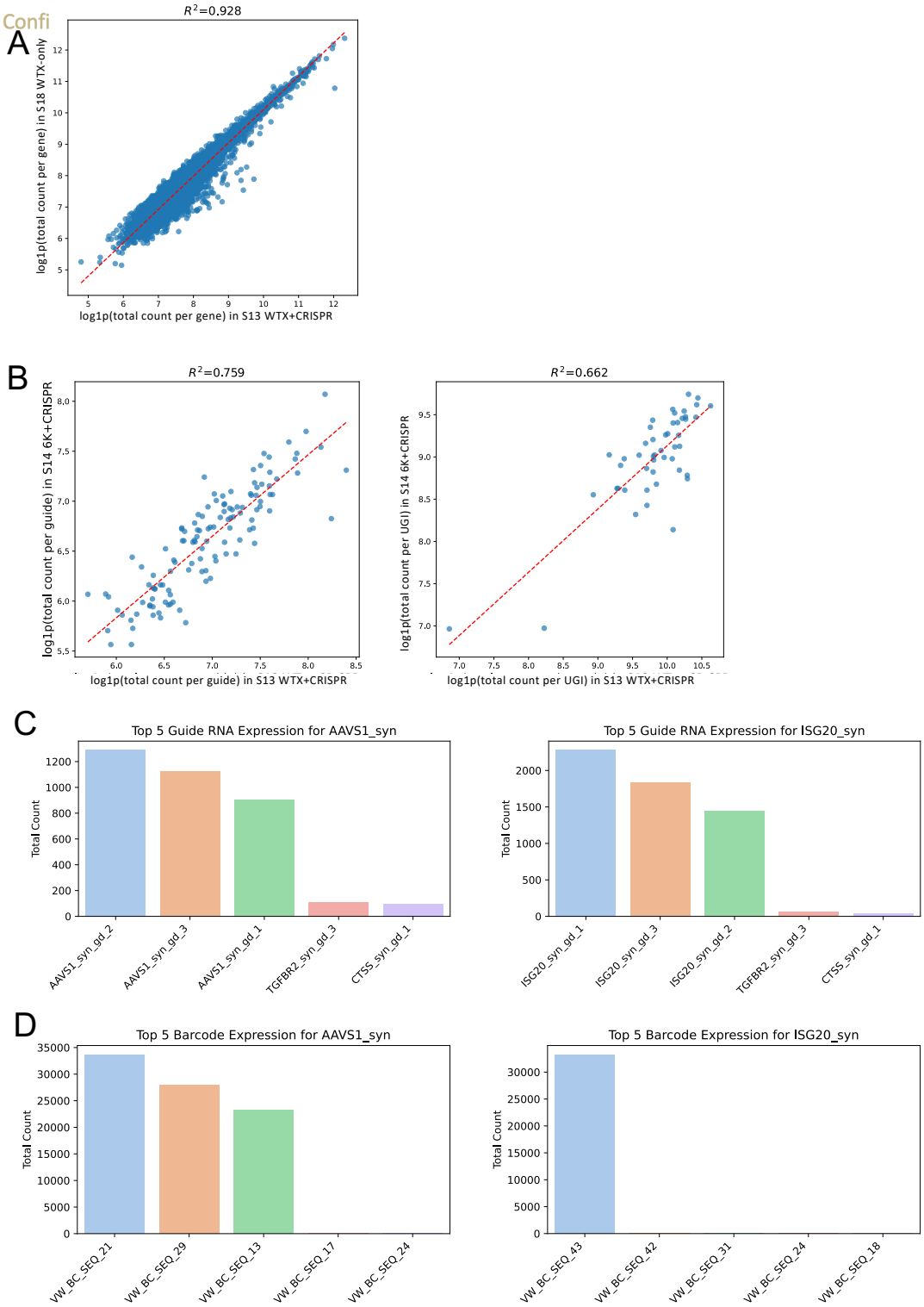

-Bruker Confidential-

-Bruker Confidential-

402 Figure S4: SPACE assay performance with WTX RNA panel

403 A: Gene expression correlation between WTX+CRISPR experiment (x axis) and WTX-only experiment
404 (y axis).

405 B: Correlation of detected CRISPR molecule count between WTX+CRISPR (x axis) and 6K+CRISPR (y
406 axis). Left: gRNA count correlation; right: UGI count correlation.

407 C: Total counts per spheroid of the top 5 most abundant gRNAs in selected spheroid. Left: *AAVS1*-KO
408 spheroids; right: *ISG20*-KO spheroids.

409 D: Total counts per spheroid of the top 5 most abundant UGIs in selected spheroid. Left: *AAVS1*-KO
410 spheroids; right: *ISG20*-KO spheroids.

411

-Bruker Confidential-

Figure S5

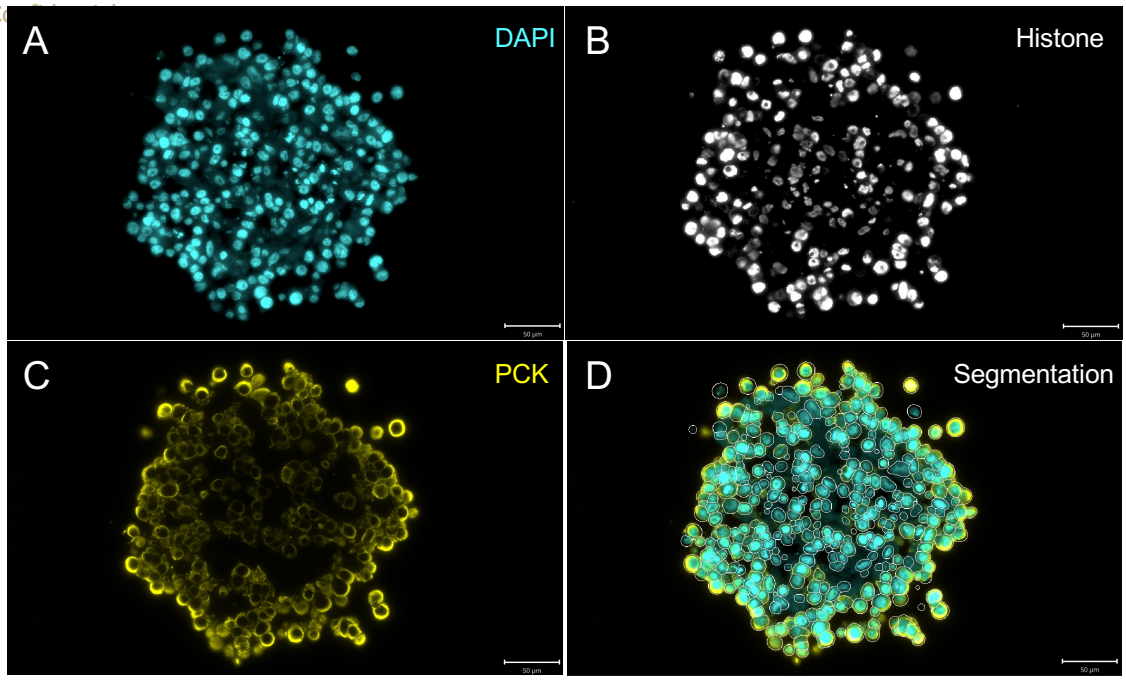

Figure S5: Example of cell segmentation

Channels of DAPI, histone and PanCK protein staining were used for segmentation.

A: DAPI.

B: Histone.

C: PanCK.

D: Composite with segmentation mask shown.

Scale bar: 50 µm.

-Bruker Confidential-

Figure S6

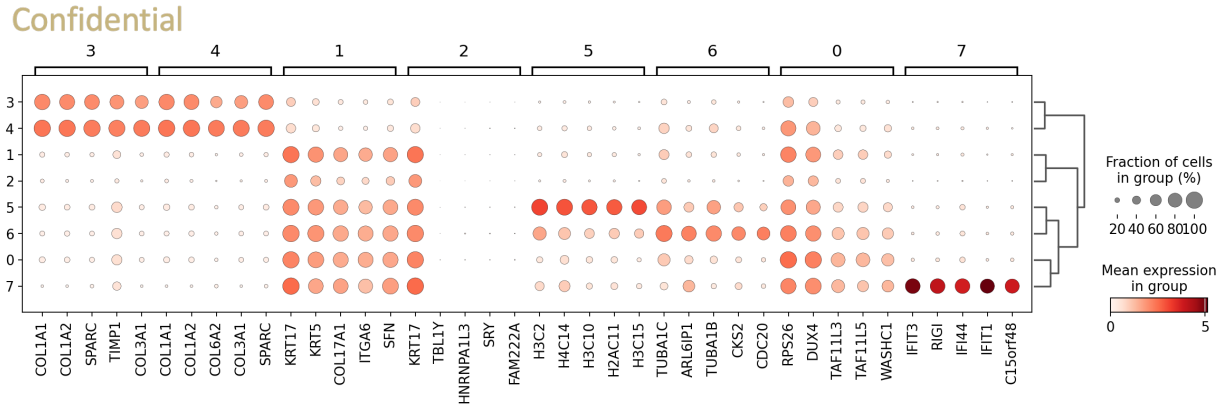

Figure S6: Cell type clustering of CAF-tumor spheroid

Expression level of marker genes in each cluster.

-Bruker Confidential-

Figure S7

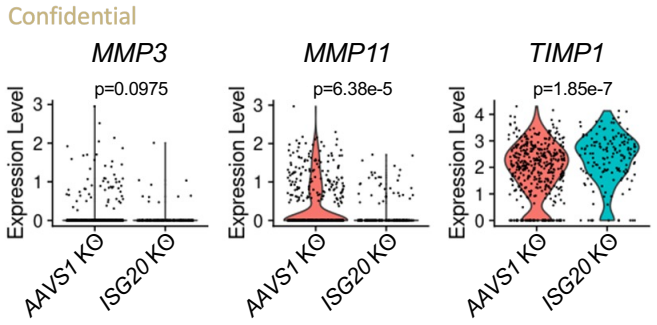

Figure S7: MMP downregulation in *ISG20*- vs *AAVS1*-KO spheroids

Violin plots of selected gene expression level in CAFs in *AAVS1*-KO and *ISG20*-KO spheroids quantified from WTX+CRISPR SPACE. P values were calculated by Wilcoxon rank sum test.

-Bruker Confidential-

Figure S8

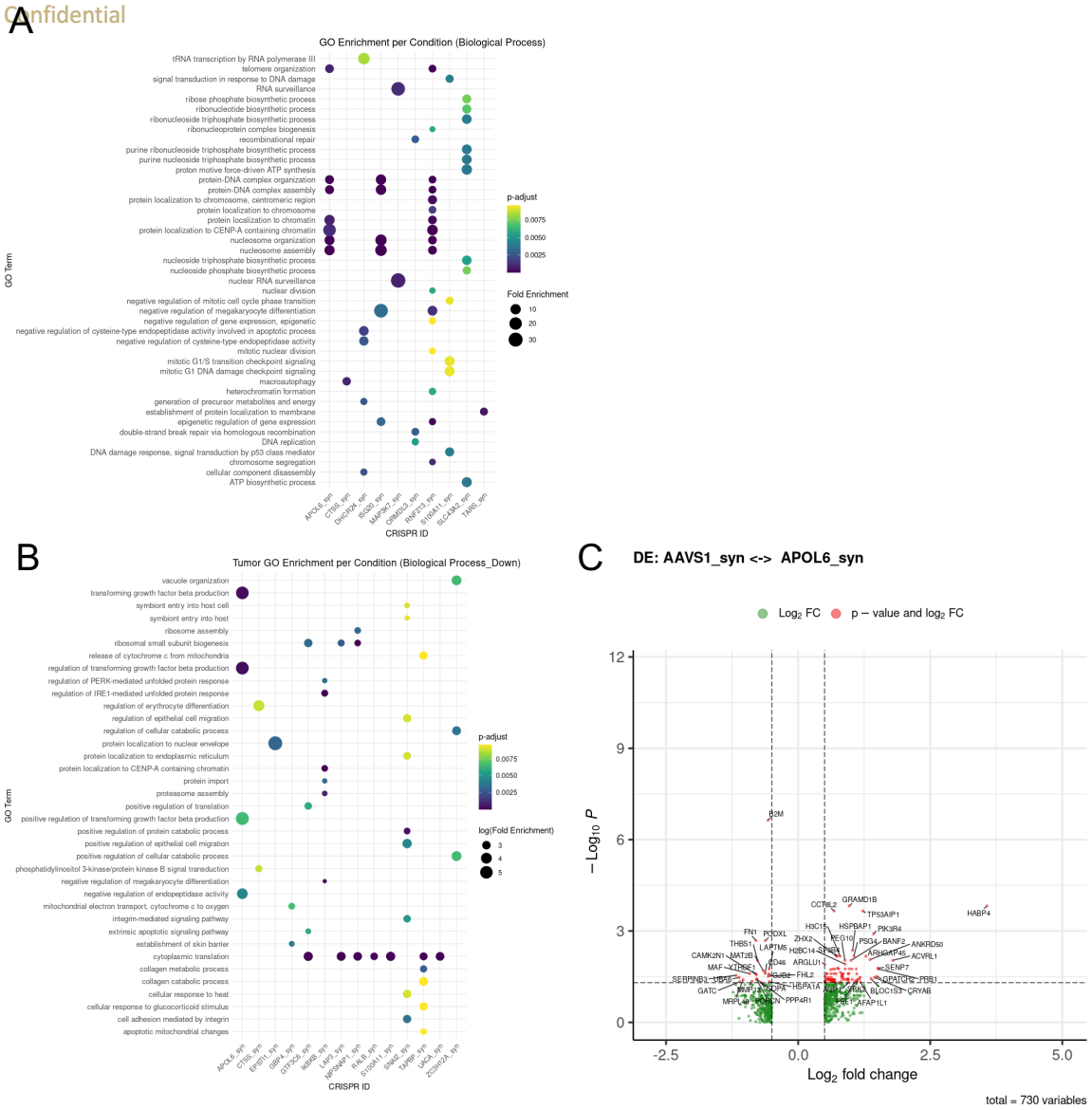

Figure S8: Differentially expressed genes in tumor

A: Enriched GO terms (biological process) of upregulated tumoral genes.

B: Enriched GO terms (biological process) of downregulated tumoral genes.

C: Volcano plot of differentially expressed genes in tumor cells of *APOL6*-KO spheroids.

-Bruker Confidential-

Figure S9

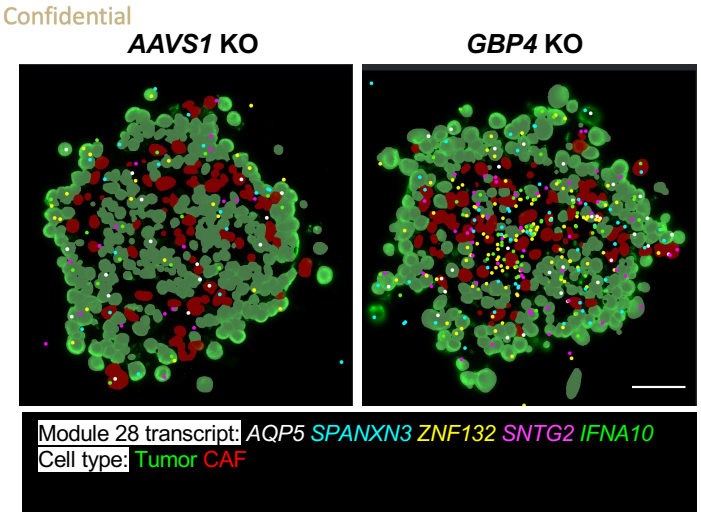

Figure S9: Spatially variable gene module in *GBP4*-KO spheroids.

Representative images from SPACE showing the RNAs of the 5-gene SVG in AAVS1-KO and GBP4-KO spheroids. Scale bar: 50 µm.

-Bruker Confidential-

Figure S10

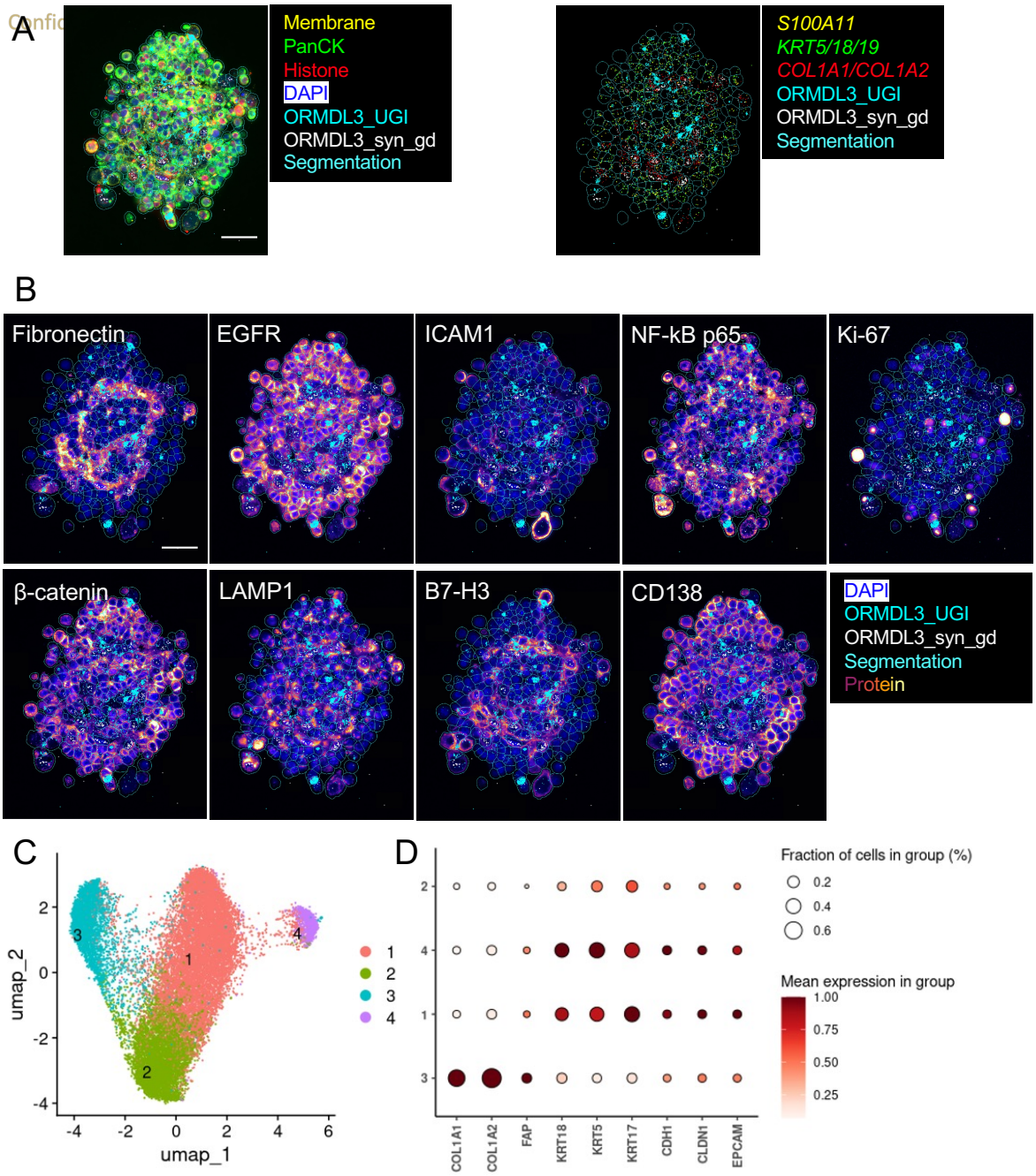

Figure S10: Multimodal SPACE

A: Representative images of RNA detection of multiomic SPACE. Selective transcripts and morphological markers for cell segmentation are shown for the same *ORMDL3*-KO spheroid. Scale bar: 50 µm.

B: Representative images of protein detection of multiomic SPACE. Selective protein stainings are shown for the same spheroid as A. Scale bar: 50 µm.

-Bruker Confidential-

C: Cell clustering of multiomic SPACE based on endogenous mRNAs.

D: Expression level of selected marker genes across different cell clusters.

-Bruker Confidential-

Table S1

Confidential

	SPACE	Perturb-seq	Perturb-FISH	Perturb-Multi	RAEFISH
Perturbation coverage	200 (up to 2000)	Genome-wide	~ 70	~ 400	~ 500
RNA coverage	~18000 genes	Whole transcriptome	~ 130 genes	~ 200 genes	~ 300 genes
Same slide/cell protein coverage	68 (Up to 76 targets)	Not demonstrated	Not demonstrated	14	Not demonstrated
Spatial resolution	Subcellular	No spatial info	Subcellular	Subcellular	Subcellular
Model complexity	2D & 3D, FFPE compatible	Dissociated cells	Cultured cells	Fresh frozen tissues	Cultured cells

Table S1: Comparison between SPACE and other single cell/spatial perturbation technologies

-Bruker Confidential-

References

1. Feldman, D. et al. Optical Pooled Screens in Human Cells. *Cell* **179**, 787–799 e717 (2019).
2. Dhainaut, M. et al. Spatial CRISPR genomics identifies regulators of the tumor microenvironment. *Cell* **185**, 1223–1239 e1220 (2022).
3. Rood, J.E., Hupalowska, A. & Regev, A. Toward a foundation model of causal cell and tissue biology with a Perturbation Cell and Tissue Atlas. *Cell* **187**, 4520–4545 (2024).
4. Binan, L. et al. Simultaneous CRISPR screening and spatial transcriptomics reveal intracellular, intercellular, and functional transcriptional circuits. *Cell* **188**, 2141–2158 e2118 (2025).
5. Kudo, T. et al. Multiplexed, image-based pooled screens in primary cells and tissues with PerturbView. *Nat Biotechnol* **43**, 1091–1100 (2025).
6. Gu, J. et al. Mapping multimodal phenotypes to perturbations in cells and tissue with CRISPRmap. *Nat Biotechnol* **43**, 1101–1115 (2025).
7. Cheng, Y. et al. Perturb-tracing enables high-content screening of multi-scale 3D genome regulators. *Nat Methods* **22**, 950–961 (2025).
8. Saunders, R.A. et al. Perturb-Multimodal: A platform for pooled genetic screens with imaging and sequencing in intact mammalian tissue. *Cell* (2025).
9. Nath, S. & Devi, G.R. Three-dimensional culture systems in cancer research: Focus on tumor spheroid model. *Pharmacol Ther* **163**, 94–108 (2016).
10. Yang, D., Liu, J., Qian, H. & Zhuang, Q. Cancer-associated fibroblasts: from basic science to anticancer therapy. *Exp Mol Med* **55**, 1322–1332 (2023).
11. Williams, H.L. et al. Spatially Resolved Single-Cell Assessment of Pancreatic Cancer Expression Subtypes Reveals Co-expressor Phenotypes and Extensive Intratumoral Heterogeneity. *Cancer Res* **83**, 441–455 (2023).
12. Kessenbrock, K., Plaks, V. & Werb, Z. Matrix metalloproteinases: regulators of the tumor microenvironment. *Cell* **141**, 52–67 (2010).
13. Sharif, G.M. et al. Cell growth density modulates cancer cell vascular invasion via Hippo pathway activity and CXCR2 signaling. *Oncogene* **34**, 5879–5889 (2015).
14. Huang, J. et al. Extracellular matrix and its therapeutic potential for cancer treatment. *Signal Transduct Target Ther* **6**, 153 (2021).
15. Nazemi, M. & Rainero, E. Cross-Talk Between the Tumor Microenvironment, Extracellular Matrix, and Cell Metabolism in Cancer. *Front Oncol* **10**, 239 (2020).
16. Hu, Y. et al. Guanylate binding protein 4 negatively regulates virus-induced type I IFN and antiviral response by targeting IFN regulatory factor 7. *J Immunol* **187**, 6456–6462 (2011).
17. Cheon, H., Wang, Y., Wightman, S.M., Jackson, M.W. & Stark, G.R. How cancer cells make and respond to interferon-I. *Trends Cancer* **9**, 83–92 (2023).
18. Tasiheng, Y. et al. DNA hypo-methylation and expression of GBP4 induces T cell exhaustion in pancreatic cancer. *Cancer Immunol Immunother* **73**, 208 (2024).
19. Lee, S.J. et al. AQP5 expression predicts survival in patients with early breast cancer. *Ann Surg Oncol* **21**, 375–383 (2014).
20. Jiang, D. et al. Epigenetic silencing of ZNF132 mediated by methylation-sensitive Sp1 binding promotes cancer progression in esophageal squamous cell carcinoma. *Cell Death Dis* **10**, 1 (2018).